An energy and angle sampling program of secondary neutrons based on continuous-energy nuclear data

Ao Zhang[a,b], Geunyong Choi[a], Ser Gi Hong[a*], Jingen Chen[b]
[a]*Dept. of Nuclear Engineering, Hanyang University, 222 Wangsimni-ro, Seongdong-gu, Seoul, Korea*
[b]*Shanghai Institute of Applied Physics, Chinese Academy of Sciences, 2019 Jialuo-ro, Shanghai, China*
[*]*Corresponding author: hongsergi@hanyang.ac.kr*

***Keywords :** Energy and angle sampling, continuous-energy, ACE-format data, Monte Carlo

1. Introduction

Continuous-energy Monte Carlo neutron transport codes possess high simulation accuracy in reactor physics analysis. The point-wise continuous-energy data are processed from the evaluated nuclear data and then formatted into data tables for the use of Monte Carlo codes. Typically, MCNP uses ACE (A Compact ENDF) format nuclear data processed from NJOY [1]. For the neutron-induced reactions with secondary neutrons, Monte Carlo codes rely on random sampling methods for determining outgoing neutron energy and direction, which play a crucial neutron physics role in accuracy and efficiency of Monte Carlo simulations.

This work aims to construct the secondary neutron energy and direction tracking capabilities as basics for the further development of our in-house Monte Carlo neutron transport code in Hanyang University. To utilize ACE-format continuous-energy nuclear data, all ENDF angle and energy laws used in the ACE data files are supported in our newly developed program, including uncorrelated angle/energy laws, correlated angle-energy laws, and thermal scattering laws. With a given incident neutron energy, a target nucleus, and a reaction type, the secondary neutron energy and angular distributions can be generated using the program. The energy and angular sampling implementations have been verified against several well-established Monte Carlo codes by detailed comparisons, showing excellent agreements.

2. Angle and energy laws

2.1 Free-gas model data

The main parts of the ACE-format nuclear data library are evaluated based on the free-gas model, including the point-wise continuous-energy neutron-induced reaction cross sections, fission and scattering neutron angle and energy distributions, probability tables for heavy nuclides in unresolved energy region. Especially, the temperature-dependent cross section data are stored in separated files while they have same temperature-independent secondary neutron angle and energy distributions. Linear interpolation over incident neutron energy is employed in tabulated cross section grid data while multiple interpolation schemes are available in computing fission neutron yields, scattering cosines and outgoing energies.

2.1.1 Uncorrelated angle and energy laws

Uncorrelated angle and energy laws in neutron physics describe secondary outgoing neutron scattering angle mathematically independent of its energy distribution, allowing them to be sampled separately. Three angular distributions are described in the ACE manual [2], including isotropic, equiprobable scattering cosine bin, and tabular angular distributions. We found only isotropic and tabular angular distributions are used in ACE data files generated from the ENDF/B-VII.1 and ENDF/B-VIII.1 libraries by a comprehensive analysis through approximately 400 available nuclides. The equiprobable scattering cosine bin angular distribution might be used for other particles.

The ACE manual provides more than 10 types of energy laws, but not all of them are implemented in our sampling program. After completely checking ACE data files from the ENDF/B-VII.1 and ENDF/B-VIII.1 libraries, we found that all angle-uncorrelated secondary neutron energy distributions can be described by the following energy laws: level scattering (law=3), continuous tabular energy (law=4), Maxwell fission spectrum (law=7), evaporation spectrum (law=9), energy dependent Watt spectrum (law=11).

With the parsed angular or energy distribution data, a sampling algorithm is required for every angle or energy law. Here we introduce one representative sampling procedure for tabular angular distribution. Since the probability tables are dependent on incident neutron energy, the energy point index ι of utilized data is determined by a stochastic way:

$$\iota = \begin{cases} i, \xi_1 > f \\ i+1, \xi_1 \le f \end{cases} \quad f = \frac{E - E_i}{E_{i+1} - E_i}, \tag{1}$$

where E is the incident energy residing in an energy bin with a lower bound E_i and a high bound E_{i+1}. f is the probability for choosing high-bound energy point data, while ξ_1 is a random number from uniform distribution on [0, 1). The outgoing angular distribution consists of a scattering cosine grid, a PDF (Probability Density Function) table, and a CDF (Cumulative Distribution Function) table. The CDF is evaluated as

$$P(\mu) = P_{\iota,j} + \int_{\mu_{\iota,j}}^{\mu} p(\mu')d\mu', \quad (2)$$

where μ is the scattering cosine and j is its index, P and p are the CDF and PDF. Two approximations are used for the integral in Eq. (2), i.e., histogram or linear-linear schemes. Based on the analytical inversion method, the scattering cosine with histogram scheme is derived as

$$\mu = \mu_{\iota,j} + \frac{\xi_2 - P_{\iota,j}}{p_{\iota,j}}, \quad (3)$$

where ξ_2 is another random number from uniform distribution on [0,1). The corresponding formula for liner-liner scheme is expressed as

$$\mu = \mu_{\iota,j} + \frac{1}{k}\left(\sqrt{p_{\iota,j}^2 + 2k(\xi_2 - P_{\iota,j})} - p_{\iota,j}\right), k \neq 0, \quad (4)$$

where k is

$$k = \frac{p_{\iota,j+1} - p_{\iota,j}}{\mu_{\iota,j+1} - \mu_{\iota,j}}. \quad (5)$$

Following the above formulas, the scattering cosine can be sampled and used for calculating outgoing neutron direction.

2.1.2 Correlated angle-energy laws

When incident neutron energy is very high, the compound nucleus from incident neutron and target nucleus decay before reaching statistical equilibrium state. In this situation, angle and energy distributions of secondary neutron are strongly correlated. Among the ACE files from the ENDF/B-VII.1 and ENDF/B-VIII.1 libraries, the correlated distributions can be described by the Kalbach formulation (law=44), the tabulated angle-energy (law=61), and the N-body phase space (law=66) distributions. The Kalbach formulation is a powerful representation for outgoing neutron distributions in high energy reactions, applying to most of inelastic scattering reaction channels.

Here we introduce the sampling procedure using the Kalbach formulation, for which the outgoing neutron energy is firstly sampled using the tabular energy distribution (law=4). The PDF for scattering cosine follows the formula:

$$p(\mu)d\mu = \frac{A}{2sinhA}[cosh(A\mu) + Rsinh(A\mu)]d\mu, \quad (6)$$

where the tabulated data R and A are the precompound fraction and the angular distribution slope, respectively. R and A are determined based on the incident and outgoing energy bin indices by histogram or linear-linear interpolation schemes. For example, the linear-linear interpolation scheme gives

$$\begin{aligned} R &= R_{\iota,j} + \frac{E - E_{\iota,j}}{E_{\iota,j+1} - E_{\iota,j}}(R_{\iota,j+1} - R_{\iota,j}) \\ A &= A_{\iota,j} + \frac{E - E_{\iota,j}}{E_{\iota,j+1} - E_{\iota,j}}(A_{\iota,j+1} - A_{\iota,j}) \end{aligned}, \quad (7)$$

where ι and j are the index for incident and outgoing energy grid, respectively. The integral of Eq. (6) over [-1, μ] produces the CDF as

$$P(\mu) = \frac{1}{2sinhA}[sinh(A\mu) + Rcosh(A\mu) + sinhA - RcoshA]. \quad (8)$$

Using the analytical inversion method, we have

$$sinh(A\mu) + Rcosh(A\mu) = k, \quad (9)$$

where $k = (2\xi - 1)sinhA + RcoshA$. Let $x = e^{A\mu}$, we have

$$sinh(A\mu) + Rcosh(A\mu) = \frac{1+R}{2}x - \frac{1-R}{2}\frac{1}{x}. \quad (10)$$

Substituting Eq. (10) into Eq. (9), we can get

$$(1+R)x^2 - 2kx + (R-1) = 0. \quad (11)$$

ENDF manual mentions that $R \in [0,1]$, which ensures Eq. (11) always has one real and unique solution as

$$\mu = \frac{1}{A}\ln x, x = \frac{k + \sqrt{1 + k^2 - R^2}}{1+R}. \quad (12)$$

The angular distribution of the Kalbach formulation can be efficiently sampled using the Eqs. (7) and (12), while the energy distribution is sampled by a similar way of law=4.

2.2 Thermal scattering data

For low energy neutrons, the default free-gas model is not always appropriate for scattering cross sections. The kinematics of scattering can be affected by chemical bindings or crystalline Bragg edges of target materials, for which thermal scattering data represented by S(α,β) tables provide accurate descriptions. The S(α,β) cross sections include coherent and incoherent elastic scattering, and incoherent inelastic scattering. In thermal reactors, the thermal scattering data of moderator materials replace the original free-gas data for cross section calculations and secondary angle and energy sampling in thermal energy range, producing more accurate simulation results.

The coherent and incoherent elastic scattering only requires the sample of outgoing angular distribution because of energy conservation, while the incoherent inelastic scattering uses the correlated angle-energy distribution. For simplifications, here we only introduce the angle sampling procedure of the coherent elastic scattering. The scattering cosine depends on which Bragg edge scattered the incident neutron, describing by a probability

$$p(\mu_i) = s_i / \sum_j s_j \,, \tag{13}$$

where s_i is related to the crystallographic structure factors. After a Bragg edge has been sampled, the cosine of the angle of scattering is given by

$$\mu_i = 1 - \frac{2E_i}{E}, \tag{14}$$

where E_i is the energy of the Bragg edge that scattered the neutron.

2.3 Thermal motion of target nucleus

The ACE file data provides temperature-dependent cross section data and temperature-independent secondary neutron distribution data. The thermal motion of target nucleus in thermal energies presents comparable velocity with an incident neutron, making it necessary for the consideration of target thermal motions in two-body kinetics. Among reactions with secondary neutrons, only the elastic scattering needs to be accounted for target thermal motions since fission produces compound nuclei in equilibrium state and inelastic scatterings have energy thresholds several orders of magnitude higher than target kinetic energy.

To account for thermal motion of target nucleus, the first step is to sample the target velocity. The effective cross section for a target at temperature T is defined to give the same reaction rate for the stationary target nuclei as the real cross section gives for moving nuclei [3], as expressed as

$$\overline{\sigma}_T(v) = \frac{1}{v} \int dV \, v_r \sigma_0(v_r) M_T(V), \tag{15}$$

where the relative velocity v_r between incident neutron and target is $|\boldsymbol{v} - \boldsymbol{V}|$. σ_0 is the elastic scattering cross section for the stationary nuclei and M_T is the Maxwell-Boltzmann distribution of target velocities in the laboratory system. The Sampling Velocity of the Target nucleus (SVT) algorithm [4] is commonly used in most of Monte Carlo codes based on the constant elastic cross section approximation for the relative velocity. The distribution of target velocity can be determined by sampling over a mutually exclusive combination of two Gamma distributions of $\Gamma(3/2, 1)$ and $\Gamma(2,1)$ [5].

To improve accuracy losses from the constant cross section approximation, the Doppler Broadening Rejection Correction (DBRC) introduces a correction by implicitly retaining the dependence of the cross section on the relative velocity [6,7]. This is implemented by using a rejection sampling based on the SVT algorithm. The SVT sampled velocity is accepted only when a random number is smaller than the ratio of $\sigma_0(v_r)$ to the local maximum elastic scattering cross section on possible v_r. Both the SVT and DBRC algorithms were implemented in our program for sampling secondary neutron distribution in thermal energy range.

3. Verification of sampling results

All the source codes are written in C++ and the angle and energy laws are derived based on an abstract class, which provides a sampling interface for all derived classes. The secondary neutron energy and scattering cosine are obtained with given input parameters, such as incident neutron energy, target nucleus, reaction channel number. We tested the sampling program by code-to-code comparisons with some published results. Besides, a demo Monte Carlo neutron transport code has been developed based on the sampling implementations for criticality simulation checks. Note that all simulation results from our code in this work are labeled as Demo in figures and tables.

3.1 Sampling with free-gas data

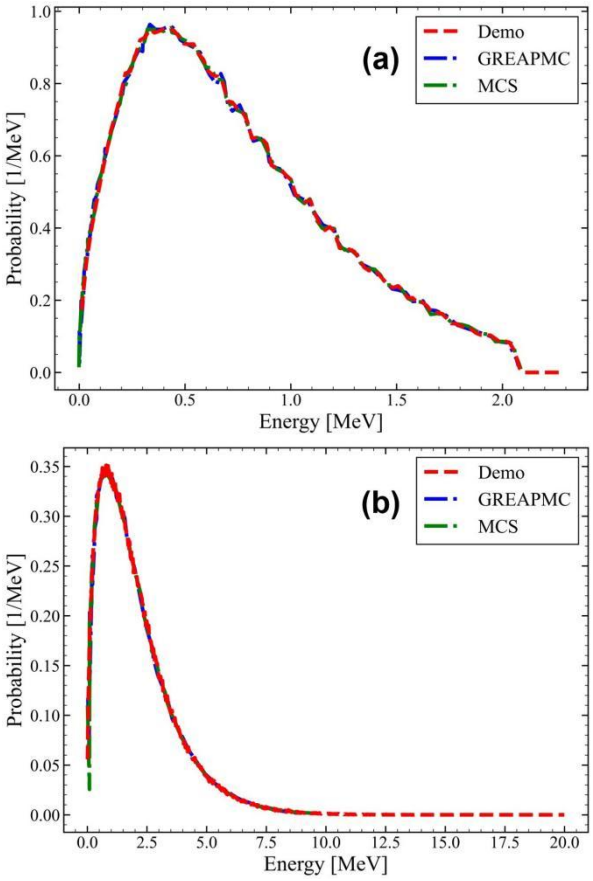

Fig. 1. Secondary neutron energy distributions for U-235 colliding with neutrons at incident energies of 2.625 MeV (a) and 0.523 MeV (b), corresponding to reaction types mt=91 and mt=18, respectively.

Fig. 1 presents the secondary neutron energy distributions for U-235 colliding with neutrons at incident energies of 2.625 MeV and 0.523 MeV, corresponding to reaction types mt=91 and mt=18,

respectively. The reference results come from MCS and GREAPMC [8] using the ENDF/B-VII.1 library. The inelastic scattering (mt=91) of U-235 uses the Kalbach formalism and its fission (mt=18) uses the correlated tabular angle-energy law. Our code shows consistent energy distributions as MCS and GREAPMC. As shown in Fig. 1, the energy distributions of mt=91 and mt=18 reactions have no strong dependencies on incident neutron energies.

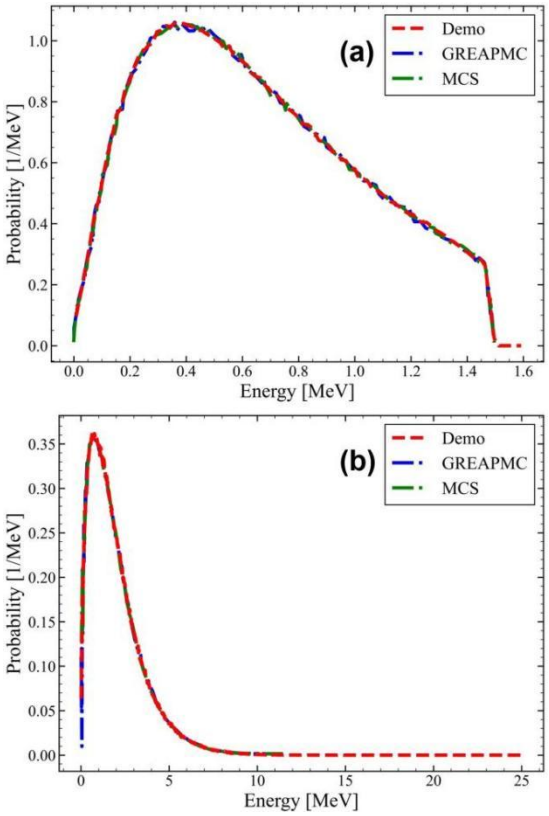

Fig. 2. Secondary neutron energy distributions for U-238 colliding with neutrons at incident energies of 2.625 MeV (a) and 1.118 MeV (b), corresponding to reaction types mt=91 and mt=18, respectively.

Similar to Fig. 1, Fig. 2 gives the sampled energy distributions for U-238 with incident neutron energies of 2.625 MeV and 1.811 MeV. Good agreements between our results and the reference results can be observed. These results in Figs. 1 and 2 prove that the individually derived sampling algorithm of the Kalbach formalism law in this study is correct.

3.2 Sampling with S(α, β) tables

Fig. 3 shows the energy and angular distributions for an incoherent inelastic scattering with H-1 in water. The target temperature is 293.6 K and the incident neutron energy is 0.99 eV, which is below the energy threshold for the application thermal scattering data instead of free-gas data. Our code shows good agreements with the reference results from OpenMC and PapillonNDL [9]. The reference codes use the ENDF/B-VIII.0 library while our work use the ENDF/B-VIII.1. A difference is observed for the sharp peak at energy distributions, caused by more refined energy bins are used in our code. These two sub-figures indicate that energy losses and forward scattering owe main probabilities during the incoherent inelastic scatter of H-1.

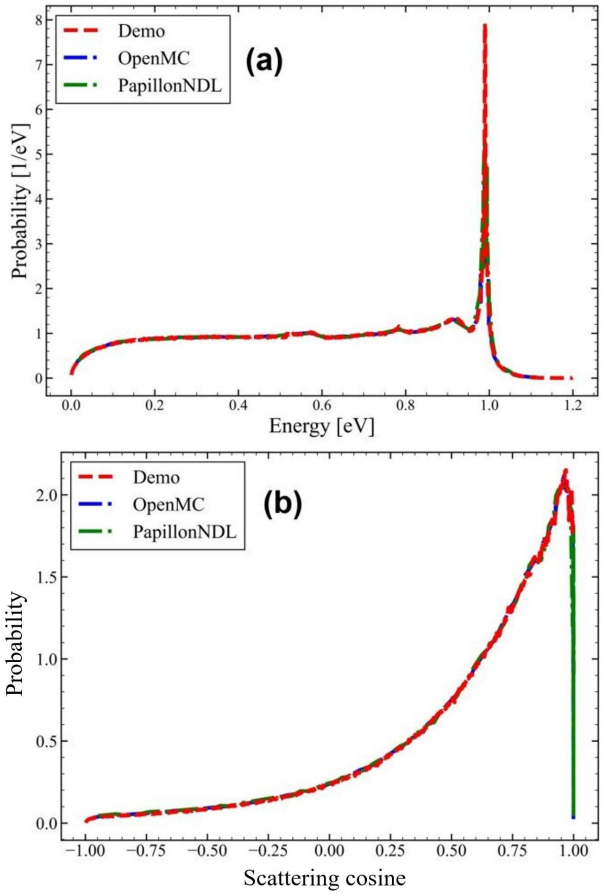

Fig. 3. Energy (a) and angular (b) distributions for an incoherent inelastic scattering with H-1 in water at 293.6 K and with an incident energy of 0.99 eV.

3.3 SVT and DBRC samplings

Fig. 4 shows the elastic scattering neutron energy distributions for U-238 colliding with an incident neutron at the energy of 36.25 eV. Both the reference SVT and DBRC sampled results come from PapillonNDL [9]. The up-scattering of neutrons can be observed due to the thermal motions of target nucleus. Compared to the SVT algorithm, the scattered neutrons with energies slightly larger than 36.25 eV have larger probabilities to be accepted in the DBRC rejection sampling, causing sharper and higher probability distribution.

Fig. 5 presents the SVT and DBRC sampled elastic scattering energy distributions for U-238 with an incident neutron energy of 36.25 eV at target temperatures of 300 K and 1000 K. Our code produces very good agreements with the reference results from

PapillonNDL [5]. With higher temperature energy, the probabilities of up-scatterings are greatly increased from the comparison of 300K and 1000K results.

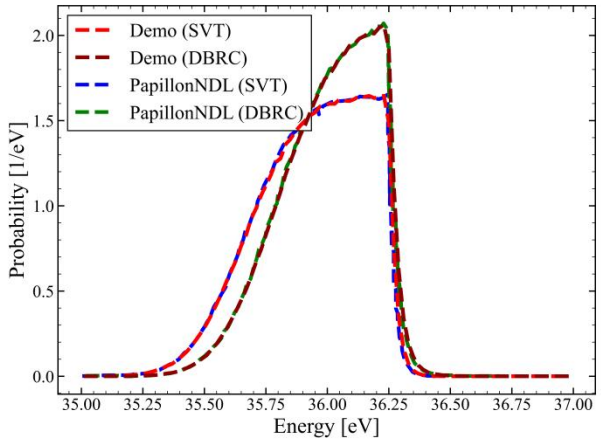

Fig. 4. Elastic scattering neutron energy distributions for U-238 with an incident neutron energy of 36.25 eV, generated with the SVT and DBRC algorithms.

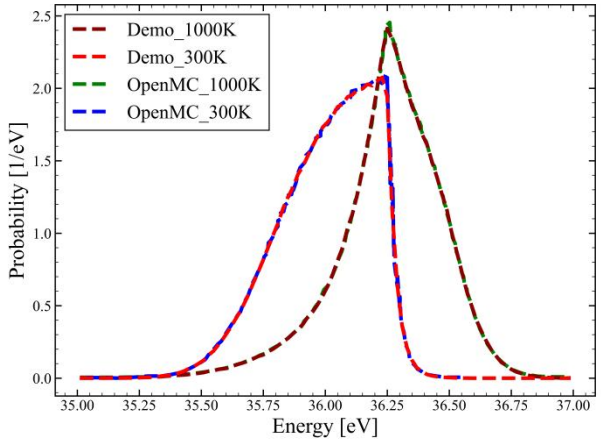

Fig. 5. SVT and DBRC sampled elastic scattering neutron energy distributions for U-238 with an incident neutron energy of 36.25 eV at target temperatures of 300 K and 1000 K.

3.4 IAEA INDC(USA)-107 benchmark

Based on the secondary distribution sampling capabilities, a demo Monte Carlo neutron transport program has been developed and verified using the IAEA INDC(USA)-107 benchmark [10]. This demo program can only treat pin cell geometry and run in sequential execution, aiming to demonstrate the neutron physics simulation capabilities.

The INDC(USA)-107 benchmark is a water-moderated UO_2 pin cell problem to verify criticality calculation accuracy in thermal system. This benchmark contains three cases with U-235 atomic enrichment increasing from 0.98% to 70%, corresponding to fuel region radius decreasing from 1.27 cm to 0.3175 cm. The square water region has a fixed length of 5.08 cm. These parameter adjustments aim to make the k_{eff} close to 1.0 for all cases. We simulate all these cases using our demo program and OpenMC, the latter of which provides references results.

Table I. Comparisons of k_{eff} between our demo code and OpenMC without thermal scattering data.

Case	OpenMC	Demo	k_{eff} diff.
1	1.01656 (11)	1.01639 (11)	-17 pcm
2	1.01334 (10)	1.01338 (14)	+4 pcm
3	1.01322 (19)	1.01323 (17)	+1 pcm

Table II. Comparisons of k_{eff} between our demo code and OpenMC with thermal scattering data.

Case	OpenMC	Demo	k_{eff} diff.
1	0.96774 (11)	0.96788 (10)	+14 pcm
2	0.92170 (12)	0.92173 (14)	+3 pcm
3	0.90897 (18)	0.90907 (17)	+10 pcm

Tables I and II give the simulated k_{eff} values from OpenMC and our demo code without and with thermal scattering data, respectively. Since the parallel computing capability is absent in our code, the number of total particle histories are set to be less than $2x10^7$ to ensure reasonable simulation time. All the k_{eff} differences from OpenMC and our demo code are smaller than 2 times of standard deviations, showing reasonable and acceptable accuracy of our newly developed program. Especially, it proves that our secondary neutron angle and energy sampling capabilities are reliable.

4. Conclusions

In this study, we developed a program with integral secondary neutron angle and energy sampling capabilities based on the ACE-format continuous-energy nuclear data. Tests on the ENDF/B-VII.1 and ENDF/B-VIII.1 show the program can parse all neutron transport required data, including thermal scattering data. The sampling results for energy laws, thermal scattering, and target thermal motions show very small differences between our code with well-established Monte Carlo codes, such as OpenMC and MCS. The criticality simulations of a UO_2 pin cell benchmark present reasonably small differences between our demo code and OpenMC, implicitly indicating the accuracy and reliability of our sampling implementations.

5. Acknowledgments

This work is supported by the Korea Institute of Energy Technology Evaluation and Planning (KETEP) grant funded by the Ministry of Trade, Industry and Energy (MOTIE) of Republic of Korea (No. RS-2025-00398867) and by the National Natural Science Foundation of China (No. 12435012).

The authors are grateful to the OpenMC development team for providing production-grade open-source

Monte Carlo source codes, which are very helpful for the authors to understand every details of computational Monte Carlo neutron transport.

REFERENCES

[1] Kulesza, J. A., et al. MCNP® code version 6.3. 0 theory & user manual. No. LA-UR-22-30006. Los Alamos National Laboratory (LANL), Los Alamos, NM (United States), 2022.
[2] Conlin, J. L., Romano, P. A compact ENDF (ACE) format specification (No. LA-UR-19-29016). Los Alamos National Laboratory (LANL), Los Alamos, NM (United States), 2019.
[3] Robert, M., et al. The njoy nuclear data processing system, version 2016. Technical report, Los Alamos National Laboratory (LANL), Los Alamos, NM (United States), 2017.
[4] Zoia, A., et al. Doppler broadening of neutron elastic scattering kernel in Tripoli-4. Annals of Nuclear Energy 54, 218 (2013).
[5] Paul, K. R., Jonathan, A. W., An improved target velocity sampling algorithm for free gas elastic scattering. Annals of Nuclear Energy, 114: 318-324, 2018.
[6] Rothenstein, W. Neutron Scattering kernels in pronounced resonances for stochastic Doppler effect calculations. Annals of Nuclear Energy, 23(4-5): 441-458, 1996.
[7] Bjorn, B. On the influence of the resonance scattering treatment in Monte Carlo codes on high temperature reactor characteristics. PhD thesis, 2010.
[8] Muhammad, R. A., et al. Development and verification of Hornet A CUDA-optimized, Monte Carlo-agnostic, continuous energy cross section processing code. Nuclear Science and Technology, 2025.
[9] Hunter B. Papillon Nuclear Data Library – a free and open-source C++/Python library for interacting with ACE files for continuous-energy neutron data. EPJ Nuclear Science & Technologies 9(23), 2023.
[10] Cullen D. E., et al. How Accurately can we Calculate Thermal Systems? United States, INDC (USA)-107: International Atomic Energy Agency; April. 2004.